Biophysical Journal
Article

Biophysical Society

Alamethicin Supramolecular Organization in Lipid Membranes from ^{19}F Solid-State NMR

Evgeniy S. Salnikov,[1] Jesus Raya,[1] Marta De Zotti,[2] Ekaterina Zaitseva,[3] Cristina Peggion,[2] Gema Ballano,[2] Claudio Toniolo,[2] Jan Raap,[4] and Burkhard Bechinger[1,*]

[1]Institute of Chemistry, University of Strasbourg/CNRS, UMR7177, Strasbourg, France; [2]ICB, Padova Unit, CNR, Department of Chemistry, University of Padova, Padova, Italy; [3]Department of Membrane Physiology and Technology, Institute of Physiology, University of Freiburg, Freiburg, Germany; and [4]Leiden Institute of Chemistry, Gorlaeus Laboratories, University of Leiden, Leiden, the Netherlands

ABSTRACT Alamethicins (ALMs) are antimicrobial peptides of fungal origin. Their sequences are rich in hydrophobic amino acids and strongly interact with lipid membranes, where they cause a well-defined increase in conductivity. Therefore, the peptides are thought to form transmembrane helical bundles in which the more hydrophilic residues line a water-filled pore. Whereas the peptide has been well characterized in terms of secondary structure, membrane topology, and interactions, much fewer data are available regarding the quaternary arrangement of the helices within lipid bilayers. A new, to our knowledge, fluorine-labeled ALM derivative was prepared and characterized when reconstituted into phospholipid bilayers. As a part of these studies, C^{19}F$_3$-labeled compounds were characterized and calibrated for the first time, to our knowledge, for ^{19}F solid-state NMR distance and oligomerization measurements by centerband-only detection of exchange (CODEX) experiments, which opens up a large range of potential labeling schemes. The ^{19}F-^{19}F CODEX solid-state NMR experiments performed with ALM in POPC lipid bilayers and at peptide/lipid ratios of 1:13 are in excellent agreement with molecular-dynamics calculations of dynamic pentameric assemblies. When the peptide/lipid ratio was lowered to 1:30, ALM was found in the dimeric form, indicating that the supramolecular organization is tuned by equilibria that can be shifted by changes in environmental conditions.

INTRODUCTION

Alamethicins (ALMs) belong to a family of antibiotic peptides (peptaibols) of fungal origin that are known to self-associate upon binding to lipid membranes (reviewed in (1–8)). The most extensively studied isoform, ALM F50/5, is characterized by a linear sequence of 19 amino acids, eight of which are α-aminoisobutyric acid residues. The peptide is acetylated at the N-terminus and the main chain is extended with a 1,2-aminoalcohol (1,2-phenylalaninol). This membrane-active peptide antibiotic is of interest as a model for more complex antimicrobial sequences, but also in analogy to larger voltage-gated channels (1,9). In electrophysiological recordings, ALM exhibits a well-defined pattern of successive increases in conductance levels, each with a duration of a few milliseconds (10,11). As many as 20 distinguishable conductance states have been described (12). The fluctuations between the stepwise K^+ and Cl^- conductivities are consistent with the various sizes of the transmembrane channels due to the presence of different oligomeric states of the helix bundles (13,14) (reviewed in (1,2)). It has been suggested that these pore structures may consist of at least three (15), four (1), or even five subunits (16). In this most widely accepted but experimentally not fully validated model, it is assumed that the polar side chains of amphipathic peptide helices are located at the center, thereby promoting the transport of polar solutes. It should be emphasized, however, that naturally occurring ALMs are poorly amphipathic, with only four (moderately) polar side chains (Gln^7, Gly^{11}, Gln^{18} (or Glu^{18}), and Gln^{19} (or Glu^{19})) facing one side of the α-helix. Of these, the two most C-terminal Gln (or Glu) residues are probably too remote from the core channel region to be directly involved in its inner lining. As a consequence, their possible role is to anchor the aggregate to the polar region of the membrane. Notably, it was reported that substitution of the polar Gln^7 by the neutral Ala reduces both the lifetime of channel opening and ion conductance, but does not completely abolish channel activity (17). Furthermore, the replacement of Gly^{11} or Pro^{14} by other, polar side chains modifies but does not abolish channel activities

Submitted April 22, 2016, and accepted for publication September 29, 2016.

*Correspondence: bechinge@unistra.fr

Editor: Mei Hong.

http://dx.doi.org/10.1016/j.bpj.2016.09.048

© 2016 Biophysical Society.

CrossMark

(18). These observations show that Gln^7 (and also Gly^{11} and Pro^{14}) are not absolutely required for ion channel formation. Finally, it is worthwhile to mention that at high concentrations of ALM and independently of transmembrane potentials, bulky ions (e.g., N^{α}-benzoyl-L-arginine-*para*-nitroanilide and carboxyfluorescein) are able to pass the membrane (19–21).

To understand the molecular mechanism of ion channel formation and membrane leakage activities, it is important to study the successive steps of membrane association, membrane insertion, the self-assembly process of channel formation, and the quaternary structure of the transmembrane array that forms the lining of an aqueous pore through which solutes permeate. Structural analyses of ALM in membrane mimetic and micellar environments indicate a high propensity for helical conformations. Based on oriented circular dichroism and solid-state NMR spectroscopies (22,23), a two-state model was proposed (1,24) in which the peptide adopts the transmembrane state above a threshold concentration. Continuous-wave electron paramagnetic resonance (EPR) studies at room temperature suggest that the majority of the membrane-bound ALM molecules are probably in the monomeric transmembrane oriented state, and upon a reduction in temperature they begin to self-assemble below the lipid-phase transition temperature (25). Ionic conductances observed at room temperature probably arise from transient and/or voltage-induced molecular associations (26). X-ray and neutron diffraction techniques have provided information about the structure factor of the pore fluid and the influence of peptides on the phase and thickness of the membrane (27–32).

Advanced pulsed EPR methods (such as pulsed electron-electron double resonance (PELDOR)) have been developed for experiments at cryogenic temperatures, and have been shown to access structural information about peptide aggregates (33,34). These techniques provide a means to measure distances between 4-amino-1-oxyl-2,2,6,6-tetramethylpiperidine-4-carboxylic acid (TOAC) spin labels in the range of 15–80 Å, and thereby allow one to obtain information about the secondary structure of a doubly labeled polypeptide. In 1,2-diacyl-*sn*-glycero-3-phosphocholine (PC) membranes, aggregated ALM molecules were found to be mostly α-helical (35). Furthermore, from a set of intermolecular distances measured between monolabeled ALMs, it was determined that the aggregate consists of a bundle of four ($n = 4.3 \pm 0.6$) parallel helices (35). However, in contrast to the general view of these ion channels, the PELDOR distances are only in agreement with a structure in which the side chains of Gln^7 face the hydrophobic lipid acyl chains rather than the pore lumen. Therefore, it is necessary to employ an independent method to investigate the arrangement of the ALM pore.

Solid-state NMR spectroscopy is a logical choice to independently test the structural arrangement of polypeptide oligomers in lipid bilayers. Magic-angle spinning (MAS) solid-state NMR techniques utilizing dipolar recoupling have been developed to measure distances between ^{13}C-isotopically labeled peptides, and the global structure can be reconstructed from the resulting data. However, most of these techniques yield only relatively short intermolecular distances (up to ~5 Å). Alternatively, one can use the centerband-only detection of exchange (CODEX) pulse sequence, which was originally designed to probe slow molecular reorientations on a timescale of ≥ 1 ms (36,37). Due to fast MAS, such experiments were initially used to reveal many heteroatomic sites with high resolution and sensitivity, and to determine their correlation times and function as well as motional amplitudes at ambient temperatures (36). When it is possible to freeze out such motion, the only mechanism of spin exchange is spin diffusion. Under such conditions, the CODEX technique allows one to elucidate the aggregate structure through distances of up to 15 Å between specifically ^{19}F-labeled residues (38,39). In the same experiment, the number of spatially clustered ^{19}F spins can also be determined on the basis of their orientational inequivalence, thereby indicating the number of subunits in the aggregate structure (N). Thus, by using this technique, one can obtain important information about the quaternary arrangement of membrane polypeptides.

The ^{19}F labeling of [$Glu(OMe)^{7,18,19}$] ALM F50/5 was achieved by synthesis of the analog ALM9, wherein the hydrophobic Val^9, situated in the middle of the sequence, was replaced by the hydrophobic and lipophobic $Dab(Tfa)^9$ residue (26,40–43). Here, we conducted a ^{19}F MAS solid-state NMR investigation of ALM9 to study its aggregation in 1-palmitoyl-2-oleoyl-*sn*-glycero-3-phosphocholine (POPC) phospholipid membranes using the CODEX approach (38). The primary structures of ALM F50/5, ALM F30/3, and ALM9 are shown in Fig. 1. The three Glu(OMe)-for-Gln substitutions do not affect the conformation and functionality of native ALM F50/5 (44–47).

MATERIALS AND METHODS

Peptide synthesis

The synthesis of ALM9 was carried out in solution according to the segment-condensation strategy described by Peggion et al. (45). In this case, Val^9 of the natural sequence was replaced by a Dab residue trifluoroacetylated at the side-chain 4-amino group. The ALM9 sample used in this study is chromatographically and chemically pure. Details regarding the synthesis and characterization of this analog and its intermediates are reported by De Zotti et al. (48).

Fluorescence dye release assays

The functionality of ALM9 was tested by measuring peptide-induced membrane leakage. Small unilamellar vesicles were prepared from 1,2-dioleyl-*sn*-glycero-3-phosphocholine (DOPC)/cholesterol (7:3) incorporating the

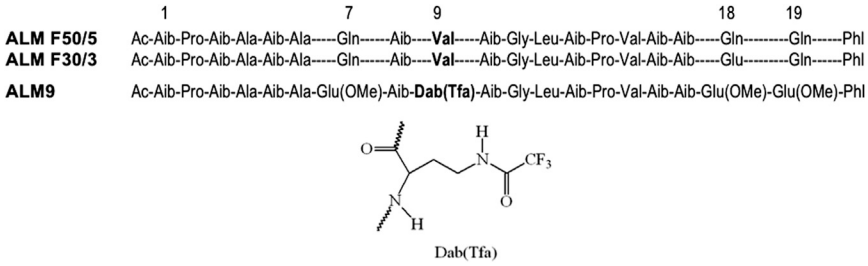

FIGURE 1 ALM peptide sequences investigated and discussed in this work.

fluorophore 5(*6*)-carboxyfluorescein (Molecular Probes, Eugene, OR) according to the procedure described by De Zotti et al. (48). Membrane-leakage experiments monitoring the lipid bilayer interactions of ALM F50/5 and ALM9 are depicted in Fig. 2.

Electrophysiological recordings

Chemicals were obtained from Sigma-Aldrich (St. Louis, MO). Lipid bilayers were formed by remote liquid spreading of a DOPC/cholesterol (7:3) solution in octane (7 mg/mL) on a MECA-16 microelectrode cavity array chip (49–51) using the Orbit-16 automated parallel bilayer platform (Nanion Technologies, Munich, Germany) as described in detail by del Rio Martinez et al. (51). Bilayer formation was controlled with the Orbit-16's internal multichannel patch-clamp amplifier (Triton-16; Tecella, Foothill Ranch, CA) running under TecellaLab (version 0.84b) software. The current traces analyzed were measured using an external Axopatch-200B patch-clamp amplifier that could be switched between channels using the Orbit's internal probe selector controlled by OrbitControl software (Nanion). The signal was filtered at a 10 kHz cutoff (four-pole Bessel filter integrated in the Axopatch) and digitized at a 100 kHz sampling rate using a NI-PCI6221 AD converter (National Instruments, Austin, TX) running under GePulse software (Michael Pusch, University of Genova, Genova, Italy). All experiments were conducted at 26°C in buffer containing 10 mM HEPES, 1 M NaCl, pH 7.4.

After formation of the lipid bilayer, the holding potential (V_{Hold}) was set to +100 mV (*trans* side). The *cis* side was set to electrical ground. The stability of the formed membranes was checked for at least 3 min. No increase in current was recorded in the controls.

ALM derivatives were dissolved in DMSO, giving a stock solution of 10 μM. Then, 0.5–1 μL of stock solution prediluted with buffer was added to the *cis* side of the measurement chamber with gentle mixing to reach a final peptide concentration of 0.1–1 nM.

Samples for solid-state NMR spectroscopy

A homogeneous mixture of POPC lipid and ALM9 (peptide/lipid molar ratio 1:13) was obtained by codissolving the membrane components in chloroform. The solution was dried first under a stream of nitrogen gas and thereafter in high vacuum overnight. The mixture was dispersed in 10 mM Tris buffer (pH 7.5) by vortex mixing. The hydrated lipid bilayers were subjected to five rapid freeze-thaw cycles, centrifuged, and concentrated by pelleting in a benchtop centrifuge. After removal of the excess buffer, multilamellar vesicles in a final water concentration of ~50% w/w were obtained.

To calibrate the interactions that occurred between trifluoromethyl functional groups during CODEX experiments, we used 3,5-bis(trifluoromethyl)benzenesulfonyl chloride (5 mol %) mixed with p-toluenesulfonyl chloride powder, and a MAS speed of 15 kHz. To obtain a homogeneous dispersion, both compounds were codissolved in methanol and left under the hood for 2 days (allowing slow evaporation of methanol). Thereafter, the condensed solution was flash-frozen in liquid nitrogen and dried under high vacuum for 2 days. The resulting white powder was then transferred into the MAS rotor. A decay constant of 1.3 ms and an equilibrium value of 0.5 were observed, resulting in the overlap integral value of 450 μs (cf. Results and Luo and Hong (38)).

Solid-state NMR spectroscopy

^{19}F solid-state NMR spectra were acquired at 470.4 MHz on an Avance wide-bore 500 NMR spectrometer (Bruker, Rheinstetten, Germany) equipped with a triple-resonance MAS 3.2 mm probe that allows simultaneous tuning of the ^{1}H and ^{19}F frequencies on a single channel through a combiner/splitter assembly. The spinning speed was set to 15 kHz. Experiments were conducted at different temperatures using cold air (see below). The typical radiofrequency field strengths were 70 kHz for ^{19}F and 50 kHz for ^{1}H. The recycle delay was 1 s. The ^{19}F chemical shifts were referenced to the Teflon ^{19}F signal at −122 ppm.

^{19}F-CODEX experiments were performed at a 15 kHz MAS speed as described by Luo and Hong (38). The normalized intensity, S/S_0, was measured as a function of the mixing time until it reached a plateau. Error bars were propagated from the signal/noise ratios of the S_0 and S spectra. The reference experiment (S_0) was conducted by using the same sample but under conditions in which spin diffusion was absent and the signal decay was governed solely by T_2 relaxation.

For temperature control, dry air at 223 K was sent from the Bruker cooling unit (BCU Xtreme) to the MAS probe. To reach 240 K for the membrane samples, the temperature was set to 226 K, since previous calibration measurements showed that 15 kHz MAS adds ~14 K at the level of the sample. Lower temperatures were obtained by constant high airflow without heating.

Data analysis

The NMR data were simulated using the ^{19}F coordinates of the ALM9 pentamer model. The latter was obtained by using the MD simulation pentamer structure of ALM F30/3 in POPC (AlmN5end.pdb) as the starting structure (the PDB structure was kindly provided by Dr. P. Tieleman). Then, the Val^{9} residues were replaced by Dab(Tfa)^{9} using HyperChem software (Hypercube, Gainesville, FL), and the distances between the CF_3-carbon nuclei of the rather flexible Dab(Tfa) side chains were further equilibrated by MD simulation for 100 ps while the peptide backbone coordinates were kept fixed. The average of the distances between the five different label positions and the average of their ^{19}F coordinates were used as input for the CODEX simulation.

RESULTS AND DISCUSSION

Peptide-induced leakage and electrophysiological recordings

The ^{19}F analog (ALM9) was tested for its ability to permeate phospholipid bilayers. Small unilamellar vesicles were prepared from DOPC/cholesterol (7:3) with

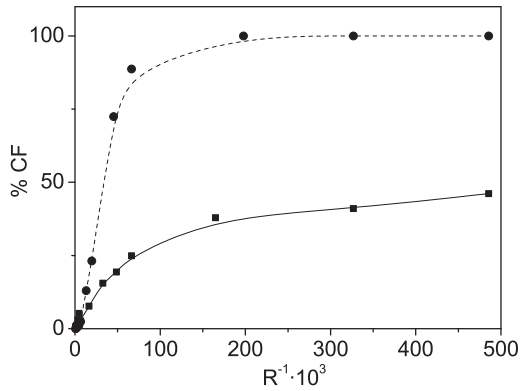

FIGURE 2 Peptide-induced leakage of 5(*6*)-carboxyfluorescein trapped within small unilamellar vesicles of DOPC/cholesterol membranes at varying ratios of P/L = [peptide]/[lipid]. The ^{19}F-analog of ALM (ALM9) (*solid squares*) and ALM F50/5 (*solid circles*) are shown. The sequences of the peptides studied are given in Fig. 1.

encapsulation of the fluorophore 5(*6*)-carboxyfluorescein (molecular weight 376). At the highest peptide/lipid ratio investigated here, the ^{19}F-analog-induced membrane leakage was about half that of ALM 50/5 (Fig. 2) or [Glu(OMe)^{7,18,19}]ALM F50/5 (not shown). As other ALM analogs (e.g., those with Gln-to-Glu(OMe) substitutions) exhibit conformations and activities that are closely related to those of native ALMs (44–47), we suggest that the limited rate of increase of membrane permeability is due to differences in pore sizes, opening times, and frequencies (1,2,52).

To better understand the different conductivities between ALM and its ^{19}F analog, we performed single-channel electrophysiological recordings. Whereas ALM F50/5 and [Glu(OMe)^{7,18,19}]ALM F50/5 exhibited closely related behaviors, in agreement with the literature (53), higher voltages were needed to observe these pore conductance levels for the ALM9 peptide (Fig. S1 in the Supporting Material). This suggests a somewhat shifted equilibrium between the open and closed states, but a closely related structure of the channels. Notably, during the structural investigations the membrane-associated peptide/lipid ratio was high, favoring the oligomeric conducting state.

Solid-state NMR spectroscopy of trifluoromethyl reference samples

The CODEX technique was originally developed to determine the number of aggregates and the intramolecular distances within the aggregated molecules, and it has been successfully applied to study the antimicrobial peptide protegrin-1 (54) and the transmembrane region of the influenza M2 protein in lipid membranes (38). The CODEX method is based on the proton-driven diffusion of ^{19}F-spin polarization under MAS conditions. This method utilizes the magnetization exchange between ^{19}F spins located at sites that consist of chemically identical molecules but are located at different spatial positions and therefore have different orientations relative to the magnetic field of the spectrometer, B_o (i.e., magnetically inequivalent sites). During the mixing time, polarization transfer occurs due to direct dipolar coupling between *n* spins in the oligomer, which allows one to extract three-dimensional (3D) structural information.

Whereas in previous investigations the ^{19}F-CODEX technique was applied to membrane-associated polypeptide complexes in which the amino acids were replaced by fluorophenyl derivatives (38,54), here we investigated ALM carrying the 4-trifluoroacetyl-2,4-diaminobutyric acid (Dab) derivative. This and other trifluoromethyl compounds should have good potential to be used within the hydrophobic anchors of membrane polypeptides or peptides in which alanine, leucine, valine, isoleucine, methionine, and α-aminoisobutyric acid are abundant. However, the dynamics and interaction properties of fluoromethyls are quite different from the previously characterized fluorophenyl, and calibration measurements have to be performed (39). Therefore, the CODEX exchange curve of bis(trifluoromethyl)benzenesulfonyl chloride (5 mol %) dispersed in *p*-toluenesulfonyl chloride powder was recorded (Fig. 3). This compound carries two fluoromethyl groups at a fixed distance of 5.5 Å (between the geometric center of three ^{19}F atoms in each CF_3 group) and allows one to experimentally determine an overlap integral of 450 μs and a plateau at 0.5. The latter value is in good agreement with a well dispersed sample in which exactly two CF_3 on the same molecule are in dipolar exchange, in contrast to a microcrystalline sample in which such contacts are abundant (39). Compared with the fluorophenyl derivative, the interactions of the magnetic moments of the two CF_3 groups are potentially higher, but at the same time are averaged by fast rotation around the C-CF_3 axis. Experimental determination of the F(0) value (38) takes into account these and other factors, and allows one to directly establish how the CODEX decay depends on the internuclear distance (Fig. 3). By homogeneously dispersing the 3,5-bis(trifluoromethyl)benzenesulfonyl compound in *p*-toluenesulfonyl chloride, one can ensure that intermolecular CF_3-CF_3 couplings are negligible, whereas such second-moment contributions exceed the nearest-neighbor interactions 43-fold in 4′-^{19}F-2′-nitroacetanilide powder (38). Notably, the much larger overlap integral of the CF_3 groups indicates that due to the cumulated interactions between two pairs of chemically equivalent ^{19}F, the range of distances can be extended in comparison with a single ^{19}F on an aromatic ring system, where F(0) is 30–40 μs and distances are typically limited to $<$15 Å (38,39).

Solid-State NMR spectroscopy of an ALM oligomer

To investigate the formation of ALM oligomers in membranes, the ALM9 analog was reconstituted into phospholipid

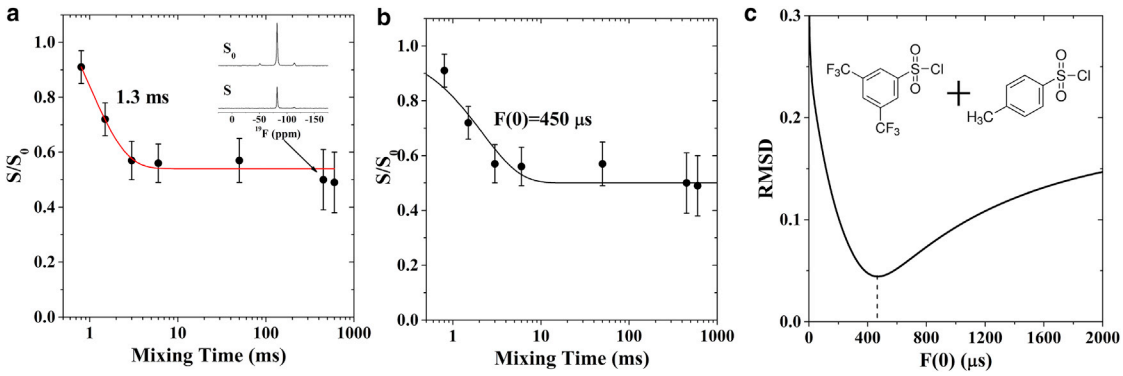

FIGURE 3 ^{19}F CODEX data of 3,5-bis(trifluoromethyl)benzenesulfonyl chloride (5 mol %) dispersed in *p*-toluenesulfonyl chloride powder at 247 K and 15 kHz MAS. (*a*) The inset shows the S_0 and S centerband intensities obtained with a mixing time of 600 ms. Unbiased S/S_0 data fitting (using an exponential decay) gives an equilibrium value of $S/S_0 = 0.54 \pm 0.04$. (*b*) Simulation of magnetization exchange data as a function of mixing time and using a simple dimer model with overlap integral value of 450 μs. (*c*) RMSD between the simulation and the experiment as a function of F(0). The inset shows the structures of 3,5-bis(trifluoromethyl)benzenesulfonyl chloride and p-toluenesulfonyl chloride. To see this figure in color, go online.

bilayers at a molar peptide/lipid ratio of 1:13 and ^{19}F solid-state NMR spectra were recorded using MAS ^{19}F-NMR. At similar concentrations, previous ^{15}N solid-state NMR experiments on ^{15}N-labeled ALM reconstituted into oriented POPC membranes indicated a transmembrane helix orientation (46,55). The high peptide/lipid ratio not only allows for direct comparison with previous NMR studies but also maximizes the ^{19}F signal intensity. Geometrical considerations indicate that even at these concentrations, on average two lipid annuli separate the monomeric transmembrane helices, and three to four layers of lipids reside between tetrameric or pentameric oligomers. With a detection limit of the ^{19}F-^{19}F CODEX experiment in the range of 15–20 Å, contributions that arise from closer proximities due to random encounters are negligible or have a comparatively small effect (see below).

To investigate the quaternary structure of ALM in POPC using the CODEX approach, we had to eliminate slow peptide motions. Therefore, in the next step, we used ^{19}F solid-state NMR spectroscopy to assess the anisotropy, and thus the motions of the labeled position, as a function of temperature. The spinning side bands of one-dimensional ^{19}F-NMR spectra of ALM9 (Fig. S2) were analyzed in quantitative detail and indicate that at 240 K and 250 K, the ^{19}F chemical-shift anisotropy is 48 ± 2 ppm and 47 ± 2 ppm (asymmetry parameter $\eta = 0$). These values are similar to the static powder limit for this label (56), whereas at temperatures of >262 K the ^{19}F chemical-shift anisotropy is reduced due to motional averaging. The change in anisotropy correlates with the freezing of membrane-associated water (57) concomitantly with the slowing down of motions of the side chains and the peptides as a whole. For comparison, a detailed analysis of the phosphatidylcholine headgroup dynamics (DMPC) as a function of temperature is of interest because it reveals that overall molecular rotation stops at the transition to the Lβ' phase (58). Thus, the Lβ' phase exhibits a crystalline character, and at the higher temperatures of this phase, molecular fluctuations occur. When the temperature is further decreased to <260 K, the free rotation around the P-O bonds is quenched and only bond librations persist (58). These data show that at <250 K, dipolar spin diffusion remains the predominant mechanism of magnetization exchange, and at the same time fast rotation of the CF_3 group makes all three fluorine atoms magnetically equivalent (59).

Fig. 4 *a* shows the time-dependent CODEX S/S_0 curve of ALM9 in POPC at a sample temperature of 240 K together with a representative set of spectra. The exchange of magnetization, S/S_0, as a function of the mixing time, τ_m, diminishes under spin exchange conditions. At long mixing times, the initial magnetization is equally distributed among the differently positioned molecules in the cluster, which reduces the CODEX echo intensity to $1/N$ (where N is the number of magnetically nonequivalent ^{19}F-nuclear spins per aggregate). Therefore, in a first analysis, the kinetic magnetization exchange (S/S_0) reaching equilibrium provides the number of N nonequivalent coordinates of the CF_3 carbon atoms (38). In the case of ALM9 oligomers, N also represents the number of subunits constituting the peptide aggregate. An excellent fit of the experimental data is obtained empirically by the biexponential function $S/S_0 = 0.186 + 0.334\ e^{-t/1ms} + 0.510\ e^{-t/200ms}$ (*solid line* in Fig. 4 *a*). The root mean-square deviation (RMSD) is 0.022 (i.e., when considering the error bars, the *solid line* perfectly matches the experimental data). The plateau value corresponds to $N = 5.3 \pm 0.4$, which therefore is consistent with a pentameric cluster of ^{19}F nuclei.

The S/S_0 curves were simulated using a 5 × 5 matrix of kinetic diffusion rate constants, which are related by $1/r^6$ to the distances r between the spatially different coordinates of the ^{19}F nuclei within the symmetric pentamer (35). Whereas the initial fast decay of the biexponential fit is characterized by a spin diffusion mechanism involving the interspin averaged distance of $r = 11.3$ Å (corresponding to a 9 Å distance between direct neighbors), an inter-^{19}F

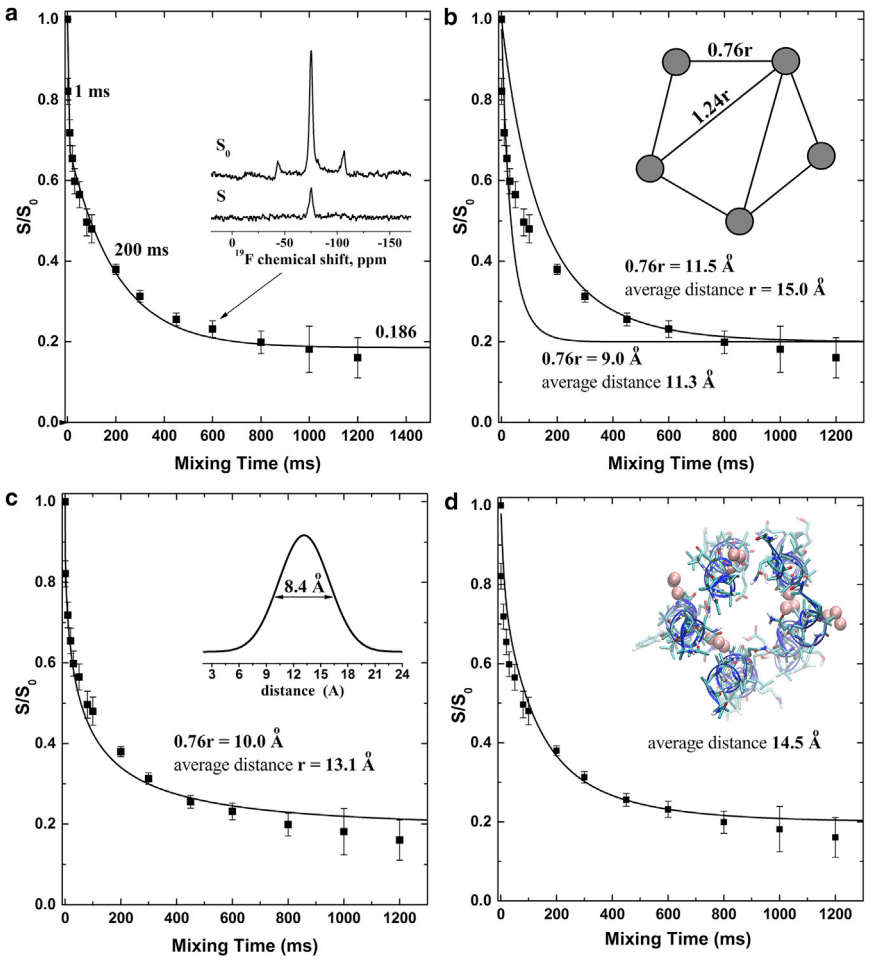

FIGURE 4 (*a*) ^{19}F CODEX data (*squares*) for ALM9 in POPC vesicles at 240 K and 15 kHz MAS. The inset shows the S_0 and S centerband intensities obtained with a mixing time of 600 ms. Model-free S/S_0 data fitting (using a biexponential) gives an equilibrium value of $S/S_0 = 0.186 \pm 0.015$ (RMSD = 0.022). The two regions dominated by fast and slow decay are labeled by their characteristic τ-values of 1 ms and 200 ms, respectively. (*b*) Simulation of magnetization exchange data as a function of mixing time and using a simple planar model of a symmetric pentamer (see *inset*). The RMSD of the $r = 15$ Å model is 0.14. (*c*) Simulation of the exchange data when a Gaussian distribution of the coordinates, and thus the mutual distances of the pentamer, are taken into consideration. The average distance between the ^{19}F-coordinates is 13.1 Å with $\sigma = 4.2$ Å (*inset*), showing a good agreement for both short and long mixing times (RMSD = 0.035). (*d*) Numerical simulations of the magnetization exchange when the ^{19}F coordinates were taken from the [Dab(TFA)$_5^9$] analog of the pentamer Alm F30-3 helix bundle obtained by MD simulation (16) (RMSD = 0.068). To see this figure in color, go online.

separation of $r = 15$ Å dominates mixing times of >50 ms (using the symmetric pentamer model; see Fig. 4 *b* for the definition of *r*). Whereas a distance of $r = 15$ Å yields an RMSD of 0.14, the deviations for shorter distances are even more pronounced. A possible reason for the biexponentiality of the curve could be structural heterogeneity or asymmetry of the spatial distribution of ^{19}F nuclei. Alternatively, good agreement with both the short and long time points of the experimental data is obtained by taking into account a Gaussian distribution of the interspin distances ($\sigma = 4.2$ Å) around an average distance of 13.1 Å (Fig. 4 *c*). The RMSD obtained with this model is 0.035.

To assess the implications of the experimentally observed intermolecular ^{19}F$\cdots^{19}$F distances for the 3D structure of the membrane-bound helix-bundle in more detail, we performed a molecular modeling experiment. This experiment was started from the published MD structure of the transmembrane pentamer in POPC bilayers (16), where the valine-9 side chain was replaced by the Dab(Tfa), which was consecutively submitted to another 100 ps MD run. For several models/snapshots created in this manner, the time-averaged spatial ^{19}F-coordinates as well as the intermolecular distances were used to simulate the CODEX data (see Materials and Methods). Fig. 4 *d* shows a pentamer model that satisfies the experimental data well (RMSD = 0.068). Furthermore, experimental data obtained at a low peptide/lipid ratio of 1:30 indicate the formation of dimers with a distance between labels of 9 Å (Fig. 5).

To estimate potential contributions from other sources and the reliability of the possible distances represented in Fig. 4, we tested alternative models. These are represented in Fig. S3, including a random distribution of monomers at low (Fig. S3 *a*) and high peptide/lipid ratios, taking into consideration a Gaussian distribution of ^{19}F-^{19}F distances (average 23 Å and $\sigma = 9.2$ Å as obtained from Monte Carlo simulations; Fig. S3 *d*). Furthermore, we estimated the effect of interpentamer contacts by calculating the CODEX decay due to a broad Gaussian distance distribution with an average of 56 Å ($\sigma = 22$ Å; Fig. S3 *c*) as obtained from the Monte Carlo simulations. Although such contributions may add to the experimental curve, none of these models alone provides a satisfactory fit of the data.

With an electric cooling system, a stable sample temperature of 240 K was obtained in the experiments shown here, each of which required many consecutive days of NMR acquisition. Even at this low temperature, it is possible

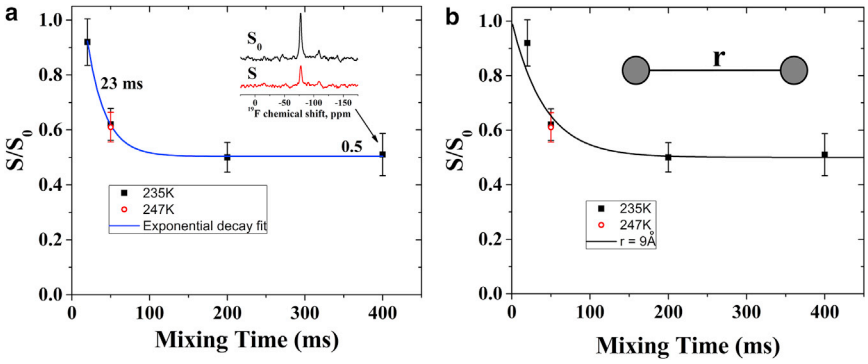

FIGURE 5 (*a*) ^{19}F-CODEX data (*squares*) for ALM9 in POPC vesicles at a peptide/lipid ratio of 1:30 and 15 kHz MAS. The inset shows the S_0 and S centerband intensities obtained with a mixing time of 400 ms. Unbiased S/S_0 data fitting (using an exponential) gives an equilibrium value of $S/S_0 = 0.50 \pm 0.045$. (*b*) Simulation of magnetization exchange data as a function of mixing time and using a simple dimer model (see *inset*). To see this figure in color, go online.

that slow motions could sufficiently modulate the chemical shift of the ^{19}F site and thereby contribute to magnetization decay (36). As a result, the measured distances would appear somewhat shorter than they really are. Therefore, the CODEX exchange was also recorded at a mix time of 50 ms, where the dipolar exchange is very sensitive to changes in molecular dynamics (MD) and temperatures of 235 K and 247 K. For this temperature range, the values of S/S_0 obtained at 50 ms are identical within experimental error (Fig. 5 *a*), indicating that slow motions were absent in the sample at 247 K, in agreement with measurements of other transmembrane helical peptides (38). Therefore, these additional measurements indicate that the observed CODEX decay is due to spin diffusion.

Aggregation model in POPC membranes

To assess the implications of the experimentally observed intermolecular ^{19}F$\cdots^{19}$F distances for the 3D structure of the membrane-bound helix bundle in more detail, we built molecular models and tested molecular arrangements that were previously determined from MD simulations (Figs. 4 and 5). The high-resolution molecular coordinates of a transmembrane pentamer arrangement that was obtained from MD simulations in POPC bilayers (16) (Fig. 4 *d*), and models of an on average symmetric pentamer with a Gaussian distribution of distances (Fig. 4 *c*) both fit the experimental data well at high peptide concentrations.

The model shown in Fig. 4 *d* represents a snapshot from an MD calculation performed on a preformed pentamer (16), which was used to obtain information about the distances between the ^{19}F-labeled Dab side chains (cf. Materials and Methods). Values for the overlap integral F(0) of 600 μs or 450 μs (cf. Fig. 3) both resulted in good fits, which indicates that within a limited range, variations of the overlap integral lead to similar results regarding the molecular structure. Other randomly selected snapshots from the MD trajectory provided acceptable representations of the experimental data, although the agreement was usually not quite as good. The Gaussian distribution of distances (Fig. 4 *c*) and the structures obtained from MD calculations (Fig. 4 *d*) agree in that considerable heterogeneity characterizes the arrangement of helices and side chains (16,55,60). Notably, the corresponding conformational fluctuations have been analyzed in terms of conductivities through the resulting pore (61).

The averaged number of ALM molecules in the oligomer in POPC is somewhat different, although within experimental error, from that obtained in previous experiments using the PELDOR technique (4.3 $\pm$ 0.6) (35), where the self-assembled structures of TOAC-spin-labeled ALM [TOAC^n,Glu(OMe)^{7,18,19}] (n = 1, 8, or 16) analogs in egg PC vesicular membranes were investigated at peptide/lipid molar ratios in the range of 1:70–1:200 and at 77 K (35,62). A lower oligomeric number could arise from the different peptide concentrations used in the PELDOR experiments, the choice of lipid fatty acyl chains (egg PC versus POPC), and the details of the amino acid side-chain compositions.

The PELDOR experiment also provides a general method for determining intermolecular distances between the nitroxide radicals of monolabeled (aggregated) molecules. Hence, it was exploited to reconstruct the tertiary arrangement of the ALM oligomers (35). According to distance-restrained MD using the PELDOR data, the long axes of the transmembrane helices are mutually tilted ($\pm 15^\circ$). Notably, the tilt angles of the helices with respect to the membrane normal of the structures shown in Fig. 4 *d* agree well with those obtained by oriented solid-state NMR of ^{15}N-labeled ALM in POPC membranes (55).

Not only is the pentamer model represented in Fig. 4 *d* highly dynamic within its own structure but the size of the supramolecular arrangement can also change over time, for example, in electrophysiological single-channel measurements where different levels in conductivity are obtained depending on the detailed experimental conditions (1,16). Indeed, when the peptide/lipid ratio is diminished, smaller oligomers predominate (Fig. 5), which could contribute to the differences between the calcein release activities observed for different ALM species and derivatives (Fig. 2) (1,2). Furthermore, the occurrence of higher-order oligomers cannot be ruled out for the more concentrated

sample when contacts between transmembrane aggregates and the error bars of these experiments are taken into account (Fig. S3). Indeed, electrophysiological recordings on ALM suggest that a number of different oligomeric states exist (1,2), and therefore one could also analyze the data by taking into account linear combinations of tetramers, pentamers, and hexamers (cf. (54)).

In this context, it is worthwhile to mention that assemblies of ALM and other membrane-active peptides have been shown to undergo a number of transitions upon membrane insertion and when localized in the membrane (63–65) (Fig. S1). In doing so, they adopt a variety of configurations and even change from in-plane to transmembrane orientations as a function of the lipid composition, membrane hydration, peptide/lipid ratio, and transmembrane voltage (1,22,23). In combination with other structural (46,55) and biophysical (1,2) data, the CODEX experiments presented here provide valuable additional information about the oligomerization size of peptides within lipid bilayers, which is difficult to obtain by other methods.

CONCLUSIONS

Here we present for the first time, to our knowledge, CODEX experiments using trifluoromethyl derivatives of a membrane-associated peptide. By experimentally calibrating the interactions between the $C^{19}F_3$ groups, we were able to better define the size of the ALM aggregates as well as the relative arrangement of the helices. The ^{19}F-labeled analog remains conductive even to large fluorophores such as carboxyfluorescein, where a dynamic equilibrium between nonconducting and conducting aggregates exists. Different labeling schemes can be envisioned that would more closely follow the structures of naturally occurring amino acids carrying methyl groups. A comparison of the structural arrangements observed by PELDOR and CODEX solid-state NMR with previous MD simulations (at 300 K) supports the view that the energetic barrier between such different states is relatively low, and that changes in membrane composition, temperature, hydration, or buffer composition may also modulate the detailed properties of the pores. The data suggest that at room temperature, peptides exhibit a rather dynamic behavior in the membrane (Figs. 4 and 5), and extend the results of previous experiments in which the aggregate size (1,2,16), membrane topology (1,22,23), detailed secondary structure (46,66), and relative alignment of the amphipathic interfaces were shown to be in exchange and regulated by environmental parameters.

SUPPORTING MATERIAL

Three figures are available at http://www.biophysj.org/biophysj/supplemental/S0006-3495(16)30882-7.

AUTHOR CONTRIBUTIONS

E.S.S. and J. Raya set up and performed the CODEX experiments, which were analyzed in detail by E.S.S. G.B. and M.D.Z. contributed equally to the peptide synthesis in solution and chromatographic analysis. Spectroscopic characterizations and membrane-leakage experiments were performed by C.P., and electrophysiological recordings and analysis were performed by E.Z. C.T. was responsible for overall supervision of the chemical part of the project. J. Raap contributed to the simulations and discussion of the results. B.B. was responsible for the NMR experiments; discussion, planning, and coordination of the project; and writing the manuscript.

ACKNOWLEDGMENTS

We thank Jerôme Hirschinger for a valuable discussion about theoretical aspects of the experiments performed here.

This work was supported in part by the International Research Training Group "Soft Matter Science: Concepts for the Design of Functional Materials" and the German-French-University exchange program (DFA/UFA). First single-channel measurements were performed during the electryophysiology workshop at the Joint meeting of the French and German biophysical societies, Bad Herrenalb, April 11–14, 2016. It was also supported by financial contributions from the Agence Nationale de la Recherche (projects ProLipIn 10-BLAN-731, membraneDNP 12-BSV5-0012, MemPepSyn 14-CE34-0001-01, and LabEx Chemistry of Complex Systems 10-LABX-0026_CSC), the University of Strasbourg (incl. IDEX), the Centre National de Recherche Scientifique, the Région Alsace, and the RTRA International Center of Frontier Research in Chemistry. J.Raap was supported by The Netherlands Organization of Scientific Research (grant 047.017.034). M.D.Z., C.P., G.B., and C.T. received a grant from the Ministry for University and Research of Italy (PRIN 2008). M.D.Z. received a grant from the Ministry for University and Research of Italy (Futuro in Ricerca 2013, grant no. RBFR13RQXM).

REFERENCES

1. Sansom, M. S. 1993. Alamethicin and related peptaibols—model ion channels. *Eur. Biophys. J.* 22:105–124.
2. Bechinger, B. 1997. Structure and functions of channel-forming peptides: magainins, cecropins, melittin and alamethicin. *J. Membr. Biol.* 156:197–211.
3. Toniolo, C., and H. Brückner. 2009. Peptaibiotics: Fungal Peptides Containing α-Dialkyl α-Amino Acids. Wiley-VCD, Weinheim, Germany.
4. Kredics, L., A. Szekeres, …, B. Leitgeb. 2013. Recent results in alamethicin research. *Chem. Biodivers.* 10:744–771.
5. Futaki, S., and K. Asami. 2007. Ligand-induced extramembrane conformation switch controlling alamethicin assembly and the channel current. *Chem. Biodivers.* 4:1313–1322.
6. Leitgeb, B., A. Szekeres, …, L. Kredics. 2007. The history of alamethicin: a review of the most extensively studied peptaibol. *Chem. Biodivers.* 4:1027–1051.
7. Nagaraj, R., and P. Balaram. 1981. Alamethicin, a transmembrane channel. *Acc. Chem. Res.* 14:356–362.
8. Woolley, G. A. 2007. Channel-forming activity of alamethicin: effects of covalent tethering. *Chem. Biodivers.* 4:1323–1337.
9. Song, C., C. Weichbrodt, …, K. Zeth. 2013. Crystal structure and functional mechanism of a human antimicrobial membrane channel. *Proc. Natl. Acad. Sci. USA.* 110:4586–4591.
10. Gordon, L. G., and D. A. Haydon. 1972. The unit conductance channel of alamethicin. *Biochim. Biophys. Acta.* 255:1014–1018.
11. Vedovato, N., and G. Rispoli. 2007. A novel technique to study pore-forming peptides in a natural membrane. *Eur. Biophys. J.* 36:771–778.

12. Taylor, R. J., and R. de Levie. 1991. "Reversed" alamethicin conductance in lipid bilayers. *Biophys. J.* 59:873–879.
13. Boheim, G., and H. A. Kolb. 1978. Analysis of the multi-pore system of alamethicin in a lipid membrane. I. Voltage-jump corrent-relaxation measurements. *J. Membr. Biol.* 38:99–150.
14. Hall, J. E., I. Vodyanoy, …, G. R. Marshall. 1984. Alamethicin. A rich model for channel behavior. *Biophys. J.* 45:233–247.
15. Hanke, W., and G. Boheim. 1980. The lowest conductance state of the alamethicin pore. *Biochim. Biophys. Acta.* 596:456–462.
16. Tieleman, D. P., B. Hess, and M. S. Sansom. 2002. Analysis and evaluation of channel models: simulations of alamethicin. *Biophys. J.* 83:2393–2407.
17. Asami, K., T. Okazaki, …, Y. Nagaoka. 2002. Modifications of alamethicin ion channels by substitution of Glu-7 for Gln-7. *Biophys. J.* 83:219–228.
18. Kaduk, C., M. Dathe, and M. Bienert. 1998. Functional modifications of alamethicin ion channels by substitution of glutamine 7, glycine 11 and proline 14. *Biochim. Biophys. Acta.* 1373:137–146.
19. He, K., S. J. Ludtke, …, H. W. Huang. 1996. Mechanism of alamethicin insertion into lipid bilayers. *Biophys. J.* 71:2669–2679.
20. Kropacheva, T. N., and J. Raap. 2007. Enzymatic reaction in a vesicular microreactor: peptaibol-facilitated substrate transport. *Chem. Biodivers.* 4:1388–1394.
21. De Zotti, M., B. Biondi, …, C. Toniolo. 2012. Trichogin GA IV: a versatile template for the synthesis of novel peptaibiotics. *Org. Biomol. Chem.* 10:1285–1299.
22. Huang, H. W., and Y. Wu. 1991. Lipid-alamethicin interactions influence alamethicin orientation. *Biophys. J.* 60:1079–1087.
23. Salnikov, E., C. Aisenbrey, …, B. Bechinger. 2010. Solid-state NMR approaches to measure topological equilibria and dynamics of membrane polypeptides. *Biochim. Biophys. Acta.* 1798:258–265.
24. Huang, H. W. 2006. Molecular mechanism of antimicrobial peptides: the origin of cooperativity. *Biochim. Biophys. Acta.* 1758:1292–1302.
25. Bartucci, R., R. Guzzi, …, D. Marsh. 2008. Backbone dynamics of alamethicin bound to lipid membranes: spin-echo electron paramagnetic resonance of TOAC-spin labels. *Biophys. J.* 94:2698–2705.
26. Marsh, D., M. Jost, …, C. Toniolo. 2007. Lipid chain-length dependence for incorporation of alamethicin in membranes: electron paramagnetic resonance studies on TOAC-spin labeled analogs. *Biophys. J.* 92:4002–4011.
27. Huang, P., and G. H. Loew. 1995. Interaction of an amphiphilic peptide with a phospholipid bilayer surface by molecular dynamics simulation study. *J. Biomol. Struct. Dyn.* 12:937–956.
28. Keller, S. L., S. M. Gruner, and K. Gawrisch. 1996. Small concentrations of alamethicin induce a cubic phase in bulk phosphatidylethanolamine mixtures. *Biochim. Biophys. Acta.* 1278:241–246.
29. Angelova, A., R. Ionov, …, G. Rapp. 2000. Interaction of the peptide antibiotic alamethicin with bilayer- and non-bilayer-forming lipids: influence of increasing alamethicin concentration on the lipids supramolecular structures. *Arch. Biochem. Biophys.* 378:93–106.
30. Constantin, D., G. Brotons, …, T. Salditt. 2007. Interaction of alamethicin pores in DMPC bilayers. *Biophys. J.* 92:3978–3987.
31. Qian, S., W. Wang, …, H. W. Huang. 2008. Structure of the alamethicin pore reconstructed by x-ray diffraction analysis. *Biophys. J.* 94:3512–3522.
32. Pan, J., D. P. Tieleman, …, S. Tristram-Nagle. 2009. Alamethicin in lipid bilayers: combined use of X-ray scattering and MD simulations. *Biochim. Biophys. Acta.* 1788:1387–1397.
33. Milov, A. D., A. B. Ponomarev, and Y. D. Tsvetkov. 1985. Modulation beats of signal of double electron-electron resonance in spin echo for biradical systems. *J. Struct. Chem.* 25:710–713.
34. Tsvetkov, Y. D., A. D. Milov, and A. G. Maryasov. 2008. Pulsed electron-electron double resonance (PELDOR) as EPR spectroscopy in nanometer range. *Russ. Chem. Rev.* 77:487–520.
35. Milov, A. D., R. I. Samoilova, …, J. Raap. 2009. Structure of self-aggregated alamethicin in ePC membranes detected by pulsed electron-electron double resonance and electron spin echo envelope modulation spectroscopies. *Biophys. J.* 96:3197–3209.
36. deAzevedo, E. R., W. G. Hu, …, K. Schmidt-Rohr. 1999. Centerband-only detection of exchange: efficient analysis of dynamics in solids by NMR. *J. Am. Chem. Soc.* 121:8411–8412.
37. Li, W., and A. McDermott. 2012. Investigation of slow molecular dynamics using R-CODEX. *J. Magn. Reson.* 222:74–80.
38. Luo, W., and M. Hong. 2006. Determination of the oligomeric number and intermolecular distances of membrane protein assemblies by anisotropic ^{1}H-driven spin diffusion NMR spectroscopy. *J. Am. Chem. Soc.* 128:7242–7251.
39. Gilchrist, M. L., Jr., K. Monde, …, A. E. McDermott. 2001. Measurement of interfluorine distances in solids. *J. Magn. Reson.* 152:1–6.
40. Findlay, B., G. G. Zhanel, and F. Schweizer. 2012. Investigating the antimicrobial peptide 'window of activity' using cationic lipopeptides with hydrocarbon and fluorinated tails. *Int. J. Antimicrob. Agents.* 40:36–42.
41. Naarmann, N., B. Bilgiçer, …, C. Steinem. 2006. Fluorinated interfaces drive self-association of transmembrane α helices in lipid bilayers. *Angew. Chem. Int. Ed. Engl.* 45:2588–2591.
42. Giménez, D., C. Andreu, …, G. Asensio. 2006. The introduction of fluorine atoms or trifluoromethyl groups in short cationic peptides enhances their antimicrobial activity. *Bioorg. Med. Chem.* 14:6971–6978.
43. Maisch, D., P. Wadhwani, …, A. S. Ulrich. 2009. Chemical labeling strategy with (R)- and (S)-trifluoromethylalanine for solid state ^{19}F NMR analysis of peptaibols in membranes. *J. Am. Chem. Soc.* 131:15596–15597.
44. Crisma, M., C. Peggion, …, C. Toniolo. 2007. Crystal structure of a spin-labeled, channel-forming alamethicin analogue. *Angew. Chem. Int. Ed. Engl.* 46:2047–2050.
45. Peggion, C., I. Coin, and C. Toniolo. 2004. Total synthesis in solution of alamethicin F50/5 by an easily tunable segment condensation approach. *Biopolymers.* 76:485–493.
46. Salnikov, E. S., M. De Zotti, …, B. Bechinger. 2009. Alamethicin topology in phospholipid membranes by oriented solid-state NMR and EPR spectroscopies: a comparison. *J. Phys. Chem. B.* 113:3034–3042.
47. Vedovato, N., C. Baldini, …, G. Rispoli. 2007. Pore-forming properties of alamethicin F50/5 inserted in a biological membrane. *Chem. Biodivers.* 4:1338–1346.
48. De Zotti, M., G. Ballano, …, F. Formaggio. 2014. Solution synthesis, conformational analysis, and antimicrobial activity of three alamethicin F50/5 analogs bearing a trifluoroacetyl label. *Chem. Biodivers.* 11:1163–1191.
49. Baaken, G., M. Sondermann, …, J. C. Behrends. 2008. Planar microelectrode-cavity array for high-resolution and parallel electrical recording of membrane ionic currents. *Lab Chip.* 8:938–944.
50. Baaken, G., N. Ankri, …, J. C. Behrends. 2011. Nanopore-based single-molecule mass spectrometry on a lipid membrane microarray. *ACS Nano.* 5:8080–8088.
51. del Rio Martinez, J. M., E. Zaitseva, …, J. C. Behrends. 2015. Automated formation of lipid membrane microarrays for ionic single-molecule sensing with protein nanopores. *Small.* 11:119–125.
52. Boheim, G. 1974. Statistical analysis of alamethicin channels in black lipid membranes. *J. Membr. Biol.* 19:277–303.
53. Duclohier, H., and H. Wróblewski. 2001. Voltage-dependent pore formation and antimicrobial activity by alamethicin and analogues. *J. Membr. Biol.* 184:1–12.
54. Buffy, J. J., A. J. Waring, and M. Hong. 2005. Determination of peptide oligomerization in lipid bilayers using 19F spin diffusion NMR. *J. Am. Chem. Soc.* 127:4477–4483.
55. Salnikov, E. S., H. Friedrich, …, B. Bechinger. 2009. Structure and alignment of the membrane-associated peptaibols ampullosporin A

and alamethicin by oriented ^{15}N and ^{31}P solid-state NMR spectroscopy. *Biophys. J.* 96:86–100.

56. Grage, S. L., U. H. N. Dürr, …, A. S. Ulrich. 2008. Solid state ^{19}F NMR parameters of fluorine-labeled amino acids. Part II: aliphatic substituents. *J. Magn. Reson.* 191:16–23.
57. Kodama, M., and H. Aoki. 2000. Calorimetric determination of the number of differently bound water molecules in phospholipid bilayer systems. *Netsu Sokutei.* 27:19–29.
58. Dufourc, E. J., C. Mayer, …, G. Kothe. 1992. Dynamics of phosphate head groups in biomembranes. Comprehensive analysis using phosphorus-31 nuclear magnetic resonance lineshape and relaxation time measurements. *Biophys. J.* 61:42–57.
59. Batchelder, L. S., H. Niu, and D. A. Torchia. 1983. Methyl reorientation in polycrystalline amino acids and peptides: a ^{2}H NMR spin lattice relaxation study. *J. Am. Chem. Soc.* 105:2228–2231.
60. Thøgersen, L., B. Schiøtt, …, E. Tajkhorshid. 2008. Peptide aggregation and pore formation in a lipid bilayer: a combined coarse-grained and all atom molecular dynamics study. *Biophys. J.* 95:4337–4347.
61. Kessel, A., D. P. Tieleman, and N. Ben-Tal. 2004. Implicit solvent model estimates of the stability of model structures of the alamethicin channel. *Eur. Biophys. J.* 33:16–28.
62. Milov, A. D., R. I. Samoilova, …, J. Raap. 2007. Self-aggregation of spin-labeled alamethicin in ePC vesicles studied by pulsed electron - electron double resonance. *J. Am. Chem. Soc.* 129:9260–9261.
63. Huang, H. W. 2000. Action of antimicrobial peptides: two-state model. *Biochemistry.* 39:8347–8352.
64. Bechinger, B. 2010. Membrane association and pore formation by α-helical peptides. *Adv. Exp. Med. Biol.* 677:24–30.
65. Salnikov, E. S., and B. Bechinger. 2011. Lipid-controlled peptide topology and interactions in bilayers: structural insights into the synergistic enhancement of the antimicrobial activities of PGLa and magainin 2. *Biophys. J.* 100:1473–1480.
66. Bertelsen, K., B. Paaske, …, T. Vosegaard. 2009. Residue-specific information about the dynamics of antimicrobial peptides from (1)H-(15)N and (2)H solid-state NMR spectroscopy. *J. Am. Chem. Soc.* 131:18335–18342.